Page Proof Instructions and Queries

Thank you for choosing to publish with us. This is your final opportunity to ensure your article will be accurate at publication. Please review your proof carefully and respond to the queries using the circled tools in the image below, which are available **by clicking "Comment"** from the right-side menu in Adobe Reader DC.*

Please use *only* the tools circled in the image, as edits via other tools/methods can be lost during file conversion. For comments, questions, or formatting requests, please use T. Please do *not* use comment bubbles/sticky notes.

*If you do not see these tools, please ensure you have opened this file with **Adobe Reader DC**, available for free at get.adobe.com/reader or by going to Help > Check for Updates within other versions of Reader. For more detailed instructions, please see us.sagepub.com/ReaderXProofs.

Sl. No.	Query
	Please note, only ORCID iDs validated prior to acceptance will be authorized for publication; we are unable to add or amend ORCID iDs at this stage.
	Please confirm that all author information, including names, affiliations, sequence, and contact details, is correct.
	Please review the entire document for typographical errors, mathematical errors, and any other necessary corrections; check headings, tables, and figures.
	Please ensure that you have obtained and enclosed all necessary permissions for the reproduction of artworks (e.g. illustrations, photographs, charts, maps, other visual material, etc.) not owned by yourself. Please refer to your publishing agreement for further information.
	Please note that this proof represents your final opportunity to review your article prior to publication, so please do send all of your changes now.
	Please confirm that the acknowledgement, Funding and Conflict of Interest statements are accurate.
1	Please check the edits made to the sentence "On the other hand, the captured signal …" are correct, or edit as needed.
2	Should the phrase "decreased again from 25°C to 60°C" be "decreased again from 60°C to 25°C" in the sentences "To simulate the environmental effect …" and "The temperature was increased, decreased …"? If so, please insert the corrections in both the sentences.
3	Please check the edits made to the sentence "As in the previous section, the shown …" are correct, or edit as needed.

Considering temperature effect on robust principal component analysis orthogonal distance as a damage detector

Luis Eduardo Mujica[1] ⓘ**, Fahit Gharibnezhad[1], José Rodellar[1] and Michael Todd[2]** ⓘ

Abstract
In previous works, the authors have shown the feasibility of using classical and robust principal component analysis for damage detection on structures when ultrasonic guided waves are used. It has also been demonstrated that robust principal component analysis presents a higher probability of detection accuracy when data are corrupted. In the present work, a robust principal component analysis orthogonal distance is proposed as a new feature for damage detection strategy based on ultrasonic guided waves on structures subjected to uniform temperature changes. The effect of this temperature fluctuation on the signal propagation and also in the new feature is analyzed. Temperature compensation is applied to mitigate the effect of temperature changes on the reliability of the damage detection methodology. The proposed feature and damage detection strategy that considers these effects are tested on two structures: a laboratory scale composite plate and a large-scale complex composite that is representative of a component from an aerospace application. The promising result proves the ability of the new feature as a damage detection tool.

Introduction

There are several definitions for "damage" in structures depending on the situation.[1] Generally speaking, damage can be defined as "changes introduced into a system that adversely affect its current or future performance."[2] The term *damage* does not necessarily imply a total loss of system functionality, but rather that the system is no longer operating in its intended manner.

According to Rytter,[3] damage detection is the principal level in structural health monitoring (SHM). In Pawar and Ganguli[4] damage detection is defined as "the identification of existence of an anomalous condition in a system." Worden and Dulieu-Barton[5] defines the damage detection as a "method that gives a qualitative indication that damage might be present in the structure." Most damage detection and localization methods that have been proposed are based upon comparing monitored signals to baselines recorded from the structure prior to initiation of damage.[6] The simplest method is to subtract two signals and compute either the peak amplitude or the energy of the residual. This approach is very

effective if damage is the only factor causing the signals to change, but this is not always the case.

Various damage detection algorithms have been presented in the SHM field. As few recent examples, Zhou et al.[7] used random forest and data fusion as a tool for damage detection, and they show that using both methods provide more accuracy in comparison with random forest alone. Haynes et al.[8] suggested the likelihood ratio test as a optimal damage detector for distinguishing damaged and undamaged states of the structure. Razi et al.[9]

[1]Control, Dynamics and Applications (CoDAlab), Departament de Matemàtiques, Escola d'Enginyeria de Barcelona Est (EEBE), Universitat Politècnica de Catalunya (UPC), Barcelona, Spain
[2]Department of Structural Engineering, University of California, San Diego, San Diego, CA, USA

Corresponding author:
Luis Eduardo Mujica, Control, Dynamics and Applications (CoDAlab), Departament de Matemàtiques, Escola d'Enginyeria de Barcelona Est (EEBE), Universitat Politècnica de Catalunya (UPC), C. Eduard Maristany, 6-12, Sant Adrià de Besòs, Barcelona 08930, Spain.
Email: luis.eduardo.mujica@upc.edu

applied the empirical mode decomposition to establish an effective energy-based damage index to detect damages on the loosening of bolts in a pipeline's bolted angle joint. Nie et al.[10] proposed the vibration phase space features for damage detection. They used a new parameter based on topology changes of the phase space of vibration signals to identify structural damage. Meruane and Heylen[11] used parallel genetic algorithm as a tool to apply model-based algorithm for damage detection. They showed that the parallel counterpart is easier to implement with better numerical performance. Poddar et al.[12] used the time-reversal concept to detect damage in the structure. They tried to tune various parameters of interest to obtain the best possible reconstruction of the input signal. Mujica et al.[13] used principal component analysis (PCA), specifically Q-statistic and T^2-statistic, as indices to detect and distinguish different damage types. Finally, Gharibnezhad et al.[14] proposed to use robust PCA (ROBPCA) to minimize the false-positive detection rate. ROBPCA was compared with classical PCA by means of different tests demonstrating that the robust version is a better choice in terms of probability of detection performance, despite its higher computational cost. It was shown that the robust version is able to compress data more than its counterpart, which leads to conveying more information in the primary principal components. Furthermore, ROBPCA can detect and classify different damage scenarios in some cases where the classical method is not able.

To achieve reliable results, damage detection algorithms face different challenges. For example, environmental variation, particularly operational temperature fluctuation, is a main obstacle for developing any trustworthy damage detection algorithm. In general, temperature change can mask structural changes caused by damage. Different authors show that in the presence of changing temperature, many damage detectors are confounded by non-damaging changes, and therefore temperature compensation is a vital issue that should be considered.[6,15–17]

This work presents orthogonal distance (OD) as a damage detection feature on structures subjected to uniform operating temperature variations. As a first contribution, a robust variant of PCA is applied. Among the different ROBPCA algorithms previously compared by the authors, the most efficient (ROBPCA) was chosen.[14] Then the OD of each observation to the PCA subspace is measured, and the statistical distribution of the new feature is investigated. As a further contribution, the effect of temperature fluctuation on OD is analyzed, specifically on the probability distribution function (PDF) of the feature as well as its efficiency for damage detection. Finally, a temperature compensation method is applied to detect damage when the structure is subjected to different temperature conditions. All claims above are tested on two different structures to show the efficiency of proposed approach.

This article is structured in the following way. In the next section, the mathematical background and some review is presented on classical and robust PCA, OD, temperature effects on wave propagation, and temperature compensation. After that, the damage detection methodology based on the new feature is explained. Subsequently, two case studies are described, and the result of applying the proposed damage feature and damage detection approach on experimental setup is scrutinized. In this section, an extensive study on different aspects of temperature effect on statistical properties of the feature as well as damage detection is performed. Finally, the temperature compensation results are applied, and the article concludes with a summary discussion and conclusions.

Theoretical background

A description of classical and robust PCA and their application for damage detection is presented in this section. First, it is explained how the gathered data are organized for PCA. Next, the feature extracted from the PCA used to distinguish different patterns due to damage is discussed. Finally, the effect of the uniform temperature variations on this feature and its compensation are presented.

Data organization

Fundamentally, the sparse array ultrasosnic implementation relies on a network of piezoelectric (PZT) sensors/actuators. Analysis is conducted by "routes," defined as a path between actuator-receiver pairs. A given guided wave is applied to the structure several times through an exciting transducer (experimental trials). The responses are collected by the full matrix of receivers and arranged as equation (1).

This matrix $\mathbf{X} \in \mathcal{M}_{I \times K}(\mathbb{R})$—where $\mathcal{M}_{I \times K}(\mathbb{R})$ is the vector space of $I \times K$ matrices over $\mathbb{R}$—contains information from $K \in \mathbb{N}$ time instants and $I \in \mathbb{N}$ experimental trials. Each row vector (x_i^T) represents measurements from the sensor at a specific i th trial

$$\mathbf{X} = \begin{pmatrix} x_{11} & x_{12} & \cdots & x_{1k} & \cdots & x_{1K} \\ \vdots & \vdots & \ddots & \vdots & \ddots & \vdots \\ x_{i1} & x_{i2} & \cdots & x_{ik} & \cdots & x_{iK} \\ \vdots & \vdots & \ddots & \vdots & \ddots & \vdots \\ x_{I1} & x_{I2} & \cdots & x_{Ik} & \cdots & x_{IK} \end{pmatrix}$$
$$= \begin{pmatrix} x_1^T \\ \vdots \\ x_i^T \\ \vdots \\ x_I^T \end{pmatrix} \qquad (1)$$

Classical PCA

PCA is a powerful linear statistical transformation used commonly for dimension reduction, data de-correlation, and related tasks. The theory of PCA has been considered in Jolliffe,[18] Shlens,[19] and Smith[20] completely. However, a brief mathematical definition is presented in this section.

With a matrix of data organized as in equation (1), the covariance matrix $\mathbf{C}_X$ is calculated as follows

$$\mathbf{C_X} = \frac{1}{K-1}\mathbf{X}^T\mathbf{X} \in \mathcal{M}_{K \times K}(\mathbb{R}) \qquad (2)$$

The $\mathbf{C_X}$ is a square symmetric matrix ($K \times K$) that measures the degree of linear correlations within the data set between all possible pairs of variables (time instants). The subspaces in PCA are defined by the eigenvectors and eigenvalues of the covariance matrix as follows

$$\mathbf{C_X}\tilde{\mathbf{P}} = \tilde{\mathbf{P}}\mathbf{\Lambda} \qquad (3)$$

where the eigenvectors of $\mathbf{C_X}$ are the columns of $\tilde{\mathbf{P}}$ and the eigenvalues are the diagonal terms of $\mathbf{\Lambda}$ (the off-diagonal terms are zero). Eigenvalues reveal the active participation ("energy contribution") of the associated principal components; thus, the eigenvector with the largest associated eigenvalue conveys the linear combination of all the data with the largest quantity of uncorrelated information. Geometrically, the PCA transforms the data in the input bands from the multivariate attribute space to a new multivariate attribute space whose axes are rotated with respect to the original space. The axes (attributes) in the new space are the uncorrelated directions.

Thus, PCA effective seeks to reduce the dimensionality of the original, possibly correlated, data set $\mathbf{X}$ by choosing only a reduced number L, where $L < K$, of principal components corresponding to the L highest eigenvalues. The transformed data matrix $\mathbf{T}$ (score matrix) is the projection of the original data over the direction of the selected L principal components as

$$\mathbf{T} = \mathbf{XP} \in \mathcal{M}_{I \times L}(\mathbb{R}) \qquad (4)$$

ROBPCA

Among different robust algorithms of PCA, Hubert et al.[21] propose a methodology called ROBPCA that can handle high dimensional data. Having a matrix of data organized as equation (1), the first step would be to reduce the dimension of data to at most $K - 1$. This is specially useful when $m \geqslant n$. To do this, a singular value decomposition[22] of mean centered data can be used as

$$\mathbf{X} - \mathbf{1}\hat{\mu}_0^T = \mathbf{UDV}^T \qquad (5)$$

where $\hat{\mu}_0^T \in \mathbb{R}^K$ is the classical mean vector of variables, $\mathbf{1} \in \mathbb{R}^I$ is a vector of ones, $\mathbf{D} \in \mathcal{M}_{r_0 \times r_0}(\mathbb{R})$ is a diagonal matrix, $r_0 = \mathrm{rank}(\mathbf{X} - \mathbf{1}\hat{\mu}_0^T)$, $\mathbf{U} \in \mathcal{M}_{I \times r_0}(\mathbb{R})$ such as $\mathbf{U}^T\mathbf{U} = I_{r_0}$, $\mathbf{V} \in \mathcal{M}_{K \times r_0}(\mathbb{R})$ such as $\mathbf{V}^T\mathbf{V} = I_{r_0}$, and $I_{r_0} \in \mathcal{M}_{r_0 \times r_0}(\mathbb{R})$ is the identity matrix.

Without losing any information, we now work in the subspace spanned by the r_0 columns of $\mathbf{V}$. That is, $\mathbf{X} = \mathbf{UD} \in \mathcal{M}_{I \times r_0}$ becomes our new data matrix. It should be emphasized that this decomposition is just used as an affine transformation and not used to retain the first eigenvectors of matrix $\mathbf{X} \in \mathcal{M}_{I \times K}$ as it is not robust yet.

In the next stage, the h observation with the minimum outlying distance is found ($h < I$). To achieve this, for each observation x_i, its orthogonal outlying distance is computed as

$$outl_0(x_i) = max_{\mathbf{v} \in B} \frac{|x_i^T v - t_{MCD}(x_j^T v)|}{s_{MCD}(x_j^T v)} \qquad (6)$$

where B represents all directions through two data points, and $t_{MCD}(x_j^T v)$ and $s_{MCD}(x_j^T v)$ are the MCD (minimum covariance determinant) location and scale estimator, respectively.[23] The formulation above means that for each direction $\mathbf{v} \in B$, each observation of x_i is projected on $\mathbf{v}$ and its outlier distance is calculated, and then the h observations with smallest outlier distance are stored in the set H_0. If we consider μ_1 and S_0 as the mean and covariance matrix of the h observations in H_0, the first $k_0 \leqslant K$ principal components can be retained. This can be done by decomposition of S_0 as

$$\mathbf{S}_0 = \mathbf{P}_0\mathbf{L}_0\mathbf{P}_0^T \in \mathcal{M}_{K \times K}(\mathbb{R}) \qquad (7)$$

with $\mathbf{L} = diag(l_1, \ldots, l_r)$, $r \leqslant K$, and then selecting appropriate k_0 eigenvectors. After that, the data points are projected on the subspace spanned by the first k_0 eigenvectors of S_0 as

$$\mathbf{X}^* = (\mathbf{X} - \mathbf{1}\hat{\mu}_1^T)\mathbf{P} \in \mathcal{M}_{I \times k_0}(\mathbb{R}) \qquad (8)$$

where $\mathbf{P} \in \mathcal{M}_{k \times k_0}(\mathbb{R})$ consists of the first k_0 columns of $\mathbf{P}_0$ in equation (7).

In the third stage, the robust scatter matrix of the observations in $\mathbf{X}^*$ is estimated using MCD estimator. To do this, we need to find the specific h data points whose covariance matrix has minimal determinant. This may be achieved by applying Fast-MCD algorithm described in Rousseeuw and Van Driessen,[24] which leads to robust center and covariance matrix and finally, the robust scatter matrix as

$$\mathbf{T} = (\mathbf{X} - \mathbf{1}\hat{\mu}^T)\mathbf{P} \in \mathcal{M}_{I \times k_0}(\mathbb{R}) \qquad (9)$$
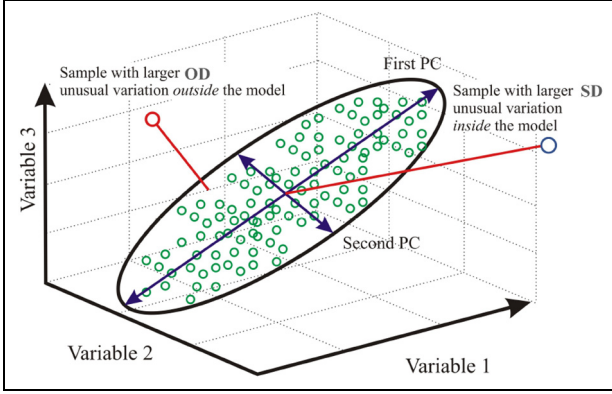
Figure 1. Different observations when a 3D data set is projected on a 2D PCA-subspace.[25]

where $\hat{\mu}$ is called robust center and $\mathbf{P} \in \mathcal{M}_{K \times k_0}(\mathbb{R})$ are robust principal components by decomposing the robust covariance matrix S of rank k_0 given by

$$\mathbf{S} = \mathbf{P} L \mathbf{P}^T \in \mathcal{M}_{K \times K}(\mathbb{R}) \qquad (10)$$

where $L \in \mathcal{M}_{k_0 \times k_0}$ is diagonal matrix with the eigenvalues $[l_1, \ldots, l_{k_0}]$.

OD as a damage feature

When data are projected on the reduced dimension PCA-subspace, they could be categorized into four types of observations.[25] For instance, Figure 1 shows the different types of observations when a three-dimensional data set is projected on a two-dimensional PCA-subspace. The first group are normal observations or regular observations (green dots) that form one homogeneous group that is close to the PCA subspace (black ellipse). The second group is a data set which lies in the same plane to the PCA space but far from the regular observations (blue dot). These observations are called *score outliers* since their score distance to the PCA subspace center SD is larger than others. The next group is called *orthogonal outliers*, whose OD to the PCA space OD is larger than others, but they are undetectable if just their projection to first or second PC are analyzed (red dot). And finally, there are data that have a larger OD and also SD to the PCA subspace than the typical projections (they are not depicted in the figure). Usually, these outliers represent data with some abnormal observations.

To distinguish between regular observations and the three types of abnormal observations for higher dimensional data, the two mentioned distances are defined as below. First, the score distance SD_i of each observation x_i is given by (called Q-statistics for other authors)

$$SD_i = \sqrt{\sum_{j=1}^{k_0} \frac{t_{ij}^2}{l_j}} \qquad (11)$$

and the OD is (called T^2-statistics for other authors)

$$OD_i = \parallel x_i - \hat{\mu} - \mathbf{P} t_i^T \parallel \qquad (12)$$

In these two equations mentioned above, t_{ij} represents the score associated to ith observation and jth dimension ($i - j$th element of $\mathbf{T}$ in equation (9)) and l_j represents the jth eigenvalue from the k_0 selected robust eigenvalues/eigenvectors. Moreover, $\hat{\mu}$ and $\mathbf{P}$ are mean and loading matrix for original data, respectively.

Temperature effect on wave propagation

Environmental and operational variability affecting the structure is one of the main obstacles for developing SHM solutions. In fact, these changes can often mask the observed changes caused by damage.[26] Among various environmental variations, uniform, "global" (meaning, assumed to affect the entire structure uniformly) temperature variations are of interest since they substantially alter the recorded waveform.[16] Generally, a small temperature change could be ignored, but significant temperature change results in a meaningful reduction of detection and classification effectiveness.

As many structures exhibit daily and seasonal temperature variations and SHM systems will need to operate across a variety of environmental conditions, understanding and considering the effect of temperature on SHM methodologies is critical. In other words, SHM systems will not be accepted in practical applications unless robust techniques are developed to explicitly account for environmental and operational constraints/conditions of the systems to be monitored.[26]

Several investigations have been performed to find out the effect of temperature in SHM methodologies, and various researchers acknowledged potential adverse effects of varying operational and environmental conditions on vibration-based or ultrasonic guided wave (UGW) damage detection.[16,27,28] In general, the main effects of the temperature variations can be categorized as follows:

- Change in the properties of PZT transducer (majority) such as PZT constants;[29,30]
- Alteration in properties of adhesive used to bond transducers to the host structure;
- Thermal expansion such as change in plate thickness, piezo dimensions, and distances traveled by the guided wave in the structure;[30]

- Change in elastic properties including density and Young module that cause changes in wave velocity.[31]

Because in general the operational thermal environment of the structure will change from test to test, the UGW measurements will reflect this variability. Therefore, those SHM methods based on a simple comparison with a unique baseline are unable to distinguish damage from benign, normal environmental and operational effects.[17]

It is certainly true that thermal gradients (e.g. localized "hot spots") are very possibly present, too. They might not affect the whole structure uniformly, and their effects on UGW propagation (and thus on damage detection) are possibly different. This article just represents an initial study into a new feature for damage detection, and therefore the current work scope is limited to test conditions and data collected in controlled, uniform temperature environments such that they can be considered a "global" condition.

Temperature compensation

Due to the influence of temperature fluctuation mentioned above, simple baseline comparison methods are unable to distinguish damage from those fluctuation effects. Different methodologies are proposed to compensate the effect of temperature such as interpolation and extrapolation of baseline,[32] baseline signal stretch (BSS),[16] or optimal baseline selection (OBS).[6,33] It should be mentioned that these techniques are valid and limited for active guided ultrasonic wave approaches.

In this work, OBS technique is applied to compensate the effect of temperature on damage detection using OD feature based on ROBPCA. In OBS technique (see Figure 2), to discriminate the effects of damage from those of environmental changes, a "bank" of baseline signals acquired at the various temperatures is
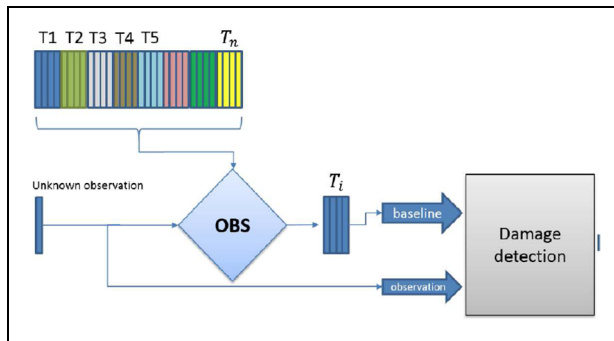
Figure 2. Schematic of OBS temperature compensation.

build. The response data (from unknown status) is compared with baseline database to find the closest match.

To achieve this goal, the baseline database should be formed at number of temperatures spanning the expected service range. In the next step, the best baseline signal is selected using appropriate measurement distance. Michaels[6] suggests three differential features which calculate the difference between the signal and the baseline. The first feature is the normalized squared error between the signal and baseline

$$E_1 = \frac{\int_0^T [y(t) - x(t)]^2 dt}{\int_0^T x(t)^2 dt} \qquad (13)$$

Here $y(t)$ is the signal and $x(t)$ is the baseline and T is the time window over which the signal are compared. The second feature is the signal difference coefficient as

$$E_2 = 1 - \frac{\int_0^T [x(t) - \mu_x][y(t) - \mu_y]}{\sigma_x \sigma_y} \qquad (14)$$

where μ is the mean and σ the standard deviation.

On the contrary to E_1, the second feature is affected only by change in the shape of the signals, not by amplitude variation. The third feature is based on the loss of local temporal coherence between the signal and baseline as

$$\gamma_{xy}(\tau, t) = \frac{R_{xy}(\tau, t)}{\sqrt{R_{xx}(0, t)R_{yy}(0, t)}} \qquad (15)$$

where $R_{xy}(\tau, t)$ is the normalized version of the short time cross correlation as

$$R_{xy}(\tau, t) = \frac{1}{\Delta T} \int_{t - \frac{\Delta T}{2}}^{t + \frac{\Delta T}{2}} x(s)w(s - t)y(s + \tau)w(s + \tau - t)ds \qquad (16)$$

where $w(t)$ is a windowing function and τ is the cross correlation lag. The loss of local coherence is the deviation of the average local coherence from unity, or

$$E_3 = 1 - \frac{1}{T} \int_0^T \max_\tau |\gamma_{xy}(\tau, t)| dt \qquad (17)$$

Damage detection strategy based on ROBPCA orthogonal distance on structures subjected to global temperature variations

As was described before, the defined distances could be used as a damage detector feature. To achieve this goal, a methodology is proposed based on OD as a damage

detection feature. At the beginning, it is necessary to collect data from the baseline condition of the structure. These data are used as a reference; the new observation (one by one) from unknown status of structure (potentially damaged) is added to the baseline to create the test data. As the majority of data in test data belong to the baseline status, the PCA space inherits its behavior from the baseline condition of the structure. Therefore, any new data that do not belong to the baseline condition is expected to have distinct OD. In this way, the OD of the any new observations from unknown status of structure is compared with the OD from data from the baseline status. This is the key-point in this algorithm that means if the new observation does not belong to the majority of data (baseline condition), then their OD is significantly different from the ODs of other observations.

In a previous work by Gharibnezhad et al.,[14] it was demonstrated that a ROBPCA is a better choice (higher probability of detection performance) for damage detection in structures when using UGW, despite its higher computational cost. Different analyses have shown that ROBPCA algorithm is the most efficient and can detect and classify different damage cases where the classical method is not able. Therefore, ROBPCA is chosen for the application in this article where the thermal environment compromise the ultrasonic data.

Figure 3 shows the described methodology. The OD calculated in this way is used as a damage feature. Since the development of a PCA model for the baseline structure has been widely and satisfactorily used by the authors, the main feature and advantage of ROBPCA is explored herein. ROBPCA is more robust against outliers, so a possible input outlier (in this case, possibly an unknown damage condition) does not affect the resulting PCA subspace, but this outlier is reflected on the projections. In conclusion, it turned out that both projections are quite similar, that is, building a "unique baseline" model or building a "baseline plus unknown data" model.

Case studies

Two case studies are considered in this article. The first setup is prepared using a carbon fiber reinforced plastic
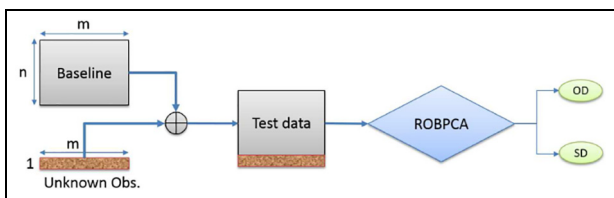
Figure 3. Damage detection methodology using OD.

(CFRP) plate equipped with microfiber composite (MFC) actuators attached on the surface of the specimen. The plate is bonded to a tubular CFRP spar. The second one is performed on a large-scale composite plate equipped with PZT transducers.

All actuation signals are generated by a National Instruments PCI − 6110 DAQ card and routed through a Krohn-Hite 7602 wideband power amplifier. Then the received waveforms are digitized with acquisition card on the same chassis with the sampling rate of 2.5 MHz.

This study employs a thermal chamber to test the effect of temperature fluctuation on wave propagation as well as the efficiency of the proposed damage feature to detect damages while temperature is changing. Due to the size limitation of the chamber, a heating lamp is used to vary temperature for the second specimen.

Case study 1: composite plate

The CFRP plate measures $305 \times 305 \times 1$ mm^2 with a lay-up of $[0/\pm45/0]$ (see Figure 4(a)). A rectangular hollow CFRP spar is bonded to the plate; this spar has an outer square diameter of 50×50 mm with a wall thickness of 6 mm. The MFC patches used for the tests were designed by Smart Material Corporation (M 2814 P2). MFC patches have an active area of 28×14 mm, with approximately 0.3 mm of thickness, and are bonded to the structure using Loctite® Hysol® E120HP. Each MFC patch is affixed to the structure ~55 mm from the spar bond line. MFC type P1 transducers are composed of PZT fibers that are uni-directionally aligned, embedded into an epoxy matrix, and sandwiched between two sets of interdigitated electrode patterns (Smart Material Corporation, Sarasota, FL). Because of their polymer-based composite design, MFC transducers are more flexible and durable than monolithic PZT transducers.[34] The transmitted signal consisted of a three-cycle tone burst with different center frequencies (100 KHz–350 KHz) and modulated by a Hanning window. Each observation is the result of exciting the structure 16 times, and its response is averaged and filtered (Butterworth bandpass filter) to reduce experimental noise.

Damages are simulated by adding mass (circular magnets 10-mm diameter) on the surface of the specimen in different locations as depicted in Figures 4(b) and (c). In all, 50 observations are recorded for the baseline structure and 25 per each damage case.

An example of a signal captured by the MFC transducers is presented in Figure 5. The signal shown corresponds to the structure in the undamaged state and is subjected to lab temperature 25°C. The time series at the top of the figure is the captured signal at route 1 → 2. As seen in Figure 4(b), the UGW does not encounter
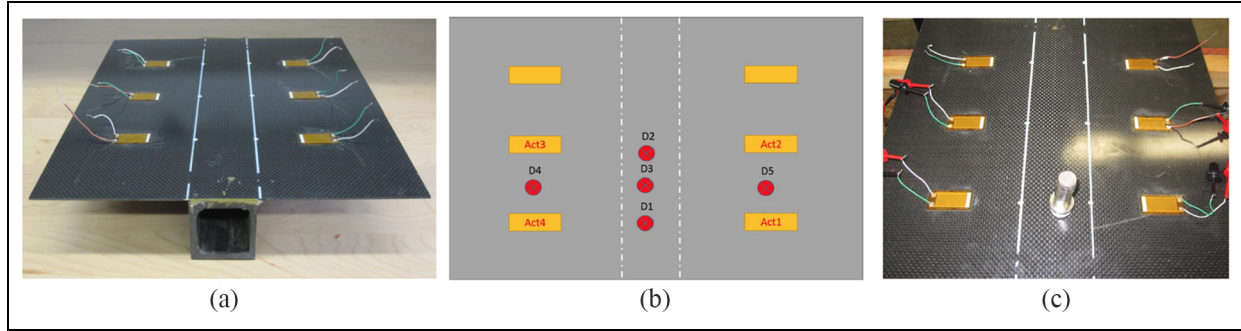
Figure 4. Case study 1, sensor and damage location: (a) snapshot, (b) schematic, and (c) seeded damage.
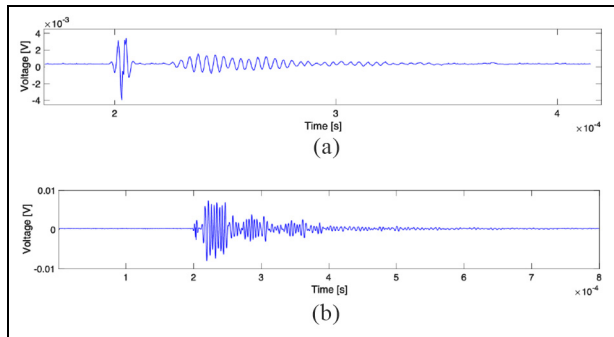
Figure 5. Example of the signal captured in two routes: (a) captured signal on route 1 → 2 and (b) captured signal on route 1 → 3.
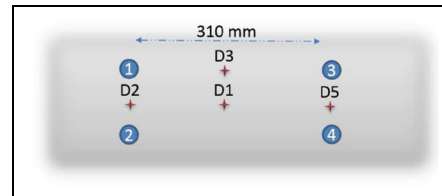

Figure 6. PZTs and damage location (schematic), case study 2.

other scattereres, and the original wavepacket arrives directly without added reflections (which arrive later).

On the other hand, the captured signal from route 1 → 3 is shown in Figure 5(b). [AQ: 1]In this case, the UGW has to cross the rectangular hollow spar, and therefore it is not easy to distinguish the principal wavepacket from the reflections.

To simulate the environmental effect, the temperature of the chamber was increased, decreased, increased again, and finally decreased again from 25°C to 60°C with the resolution of 5°C. [AQ: 2]Using a thermocouple, the ambient temperature is measured constantly. Actuation is repeated 10 times and averaged to reduce the noise effect, and 3 observations are recorded per each step temperature and damage, resulting in 96 observations in total.

Case study 2: a large-scale complex composite

The specimen that is used in this case study is a representative of a component from an aerospace structure. Although details of the structure are restricted from being published, the experimental setup and the type of signal that was captured are described as follows.

Excitation and sensing of the guided waves was performed using 2-mm diameter PZT disks attached on the surface of the structure. The transmitted signal consisted of a three-cycle tone burst, and the frequency is swept between 200 and 450 kHz. Hanning window is used to modulate signal. Each input signal is applied to the structure 10 times and then averaged and filtered (using Butterworth bandpass filter) to reduce experimental noise. The disks were bonded on the surface using *Permatex* adhesive that is robust on temperature range between −51°C and 81°C. Figure 6 shows the schematic of sensor and damage location. Damages are simulated using circular magnets attached to the surface of the structure. Every 10 received signals are averaged to construct an observation, and finally 100 observations are recorded for undamaged and 20 for each damage status of the specimen at room temperature (25°C).

To apply the temperature changes, a heating lamp is used. Experiments were performed at 25, 30, 35, 40, 45, 55, and 67°C which were measured using Raytek (RAYCMLTV) infrared thermocouple. Ten observations were gathered by each temperature and damage status.

Results and discussion

OD distribution

Although the probability density function (PDF) of OD is not used directly for damage detection in this

Table 1. Result of Lilliefors test on case study 1, different routes and status.

	1 → 2 (ND)	1 → 2 (D5)	1 → 3 (ND)	1 → 3 (D3)	1 → 4 (ND)	1 → 4 (D1)
normal	rejected	rejected	rejected	rejected	accepted	accepted
extreme	accepted	accepted	accepted	accepted	rejected	rejected
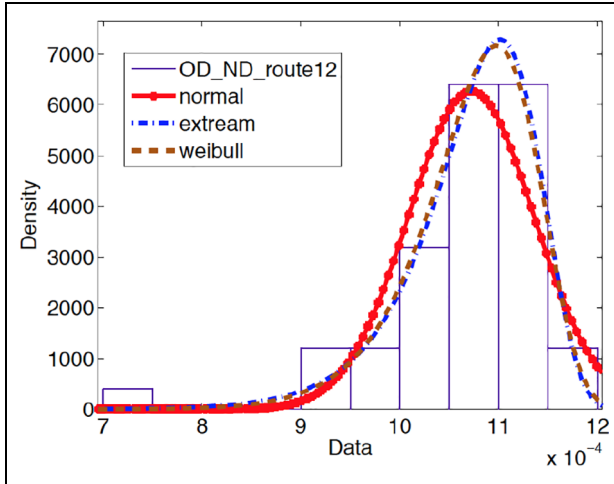
Figure 7. OD distribution, case study 1, healthy, route 1 → 2.
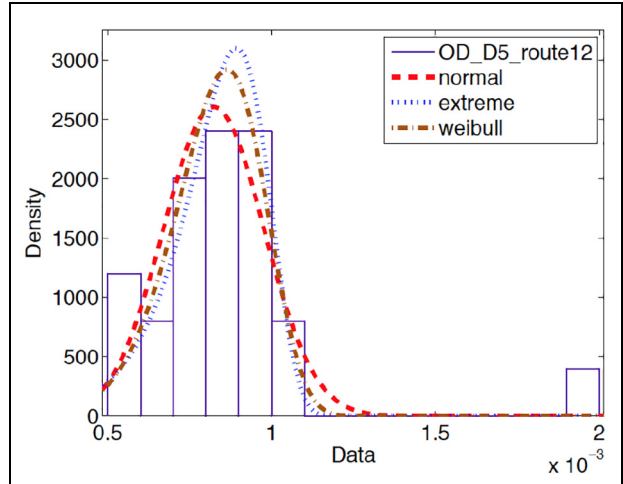
Figure 8. OD distribution, case study 1, D5, route 1 → 2.

article, it may be interesting to estimate it for future research into uncertainty quantification. As a preliminary analysis, the Lilliefors[35] test is applied on the available data gathered at 25°C from all specimen conditions: 50 observations from non-damaged case and 25 observations from each damaged case. The Lilliefors test is an alternative to a Kolmogorov–Smirnov test to check the null hypothesis that the sample in vector OD comes from a specific distribution or not. In contrast to the Kolmogorov–Smirnov test, the Lilliefors test does not require that the distribution be known.

Since the specimen is not isotropic, different routes may fit different PDFs. Therefore, the test is separately applied on different routes with a 5% significance level. It can be seen from Table 1 that, independent of the specimen condition, the null hypothesis that the OD comes from Normal distribution is rejected for routes 1 → 2 and 1 → 3, but it is accepted for route 1 → 4. Similarly, Extreme distribution is accepted for routes 1 → 2 and 1 → 3, but it is rejected for route 1 → 4.

Figures 7 to 12 show the histogram of the OD for some routes and specimen conditions. In addition, the normal, extreme value, and Weibull PDFs that fit the data are depicted. As mentioned before, non-damaged and damaged cases keep the same distribution by routes; however, in these figures it can be seen that parameters of the distribution change due to the damage. For instance, for undamaged route 1 → 2
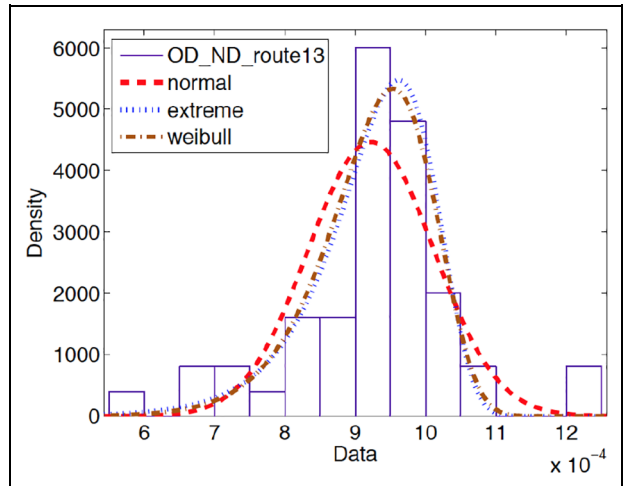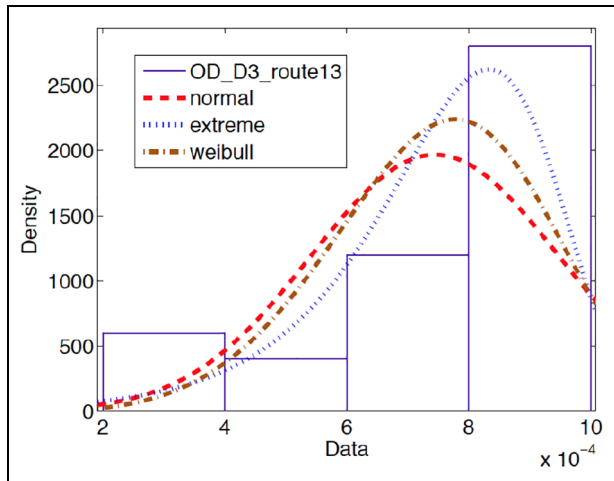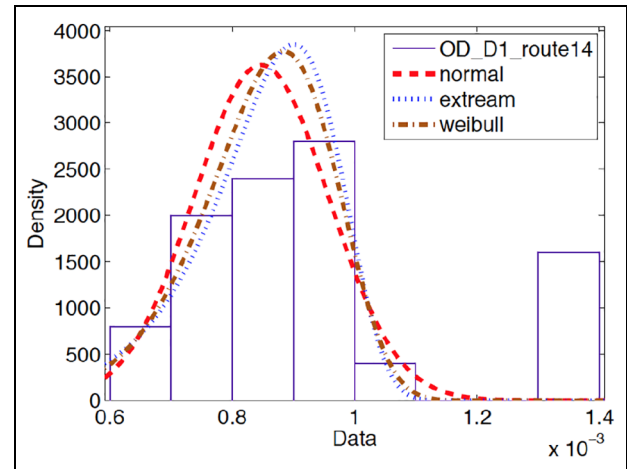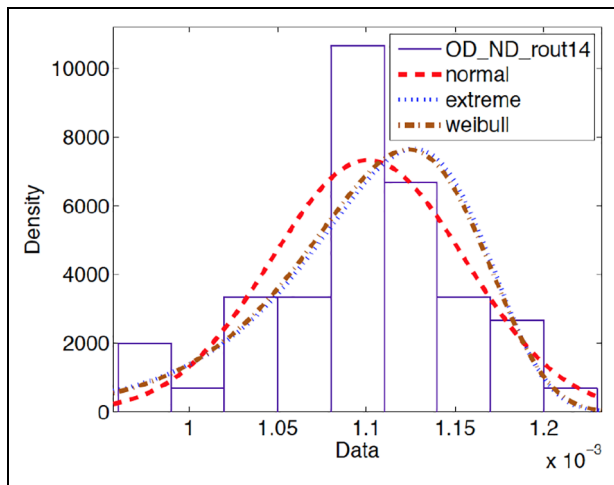

Figure 9. OD distribution, case study 1, healthy, route 1 → 3.

(Figure 7) OD follows an extreme value distribution with population mean close to 1.1×10^{-3}; however, for the same route and damage case 5 (Figure 8) the distribution is the same, but its population mean is close to 0.8×10^{-3}. The same conclusion may be obtained by comparing Figures 9 to 12.

More precisely, the moment of the OD distribution is calculated for all the routes. These moments are summarized in Table 2. It is clear that mean, median,

Table 2. OD moments.

	1 → 2 (ND)	1 → 2 (D5)	1 → 3 (ND)	1 → 3 (D3)	1 → 4 (ND)	1 → 4 (D1)
Mean	0.0011	0.00082	0.00092	0.00074	0.0011	0.00091
Median	0.0011	0.00087	0.00094	0.00081	0.0011	0.00089
Skewness	−1.73	−0.67	−0.53	−0.96	−0.43	−0.16
Kurtosis	7.71	2.57	5	2.85	3.05	2.10

Figure 10. OD distribution, case study 1, D3, route 1 → 3.

Figure 12. OD distribution, case study 1, D1, route 1 → 4.

Figure 11. OD distribution, case study 1, healthy, route 1 → 4.

skewness, and kurtosis change in presence of damage. For instance, for the undamaged route 1 → 3, these are 0.00092, 0.00094, −0.53, and 5 respectively; however for damage 3, these are 0.00074, 0.00081, −0.96, and 2.85. The same conclusion can be achieved for the rest of the routes. Although the shown results belong to case study 1, to avoid redundancies, results from case study 2 are not presented here; however, the conclusions are very similar.

Damage detection using OD

Based on the method previously mentioned, the OD is used as a damage feature to detect damage. In this section, case study 2 at room temperature (25°C) is analyzed. The available data set contains 100 observations from the undamaged specimen and 20 for each damage condition. In Figures 13 to 16, the ODs of 5 observations randomly selected by each specimen condition are shown. The rest of the observations are omitted since values are quite similar.

As is evident, OD is able to clearly distinguish between observations drawn from undamaged and damaged conditions, particularly if the damage presents as a direct scatterer on the analyzed route. For instance, by analyzing route 1 → 4, D1, which is placed on the path between these two transducers (see Figure 6), produces ODs much greater than the ODs from non-damaged, ND (see Figure 13). Similarly, D2 is clearly detected by analyzing route 1 → 2, D3 by route 1 → 3, and D5 by route 3 → 4.
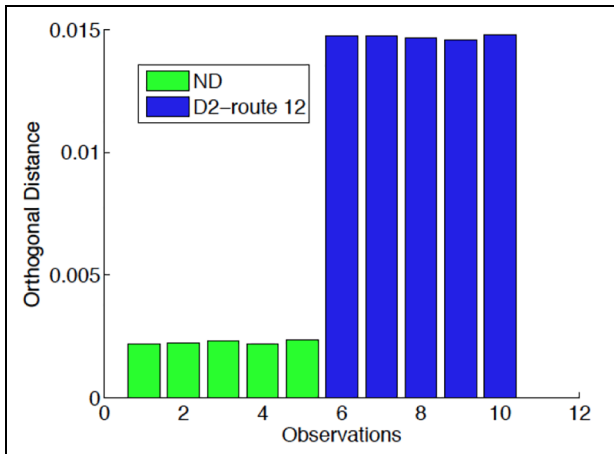
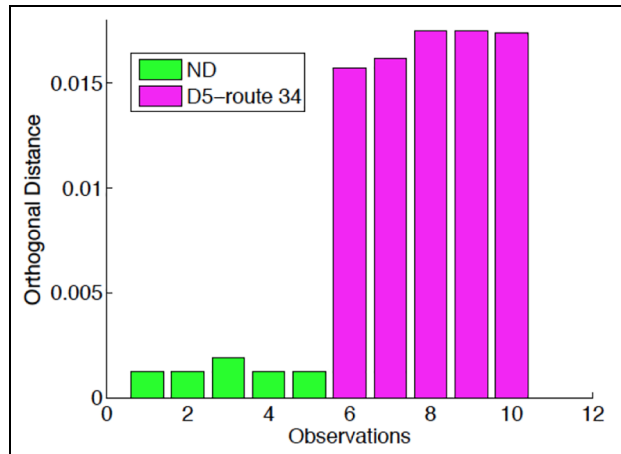Moreover, the same idea may be applied on the reverse routes, 2 → 1 instead of 1 → 2 and 3 → 1
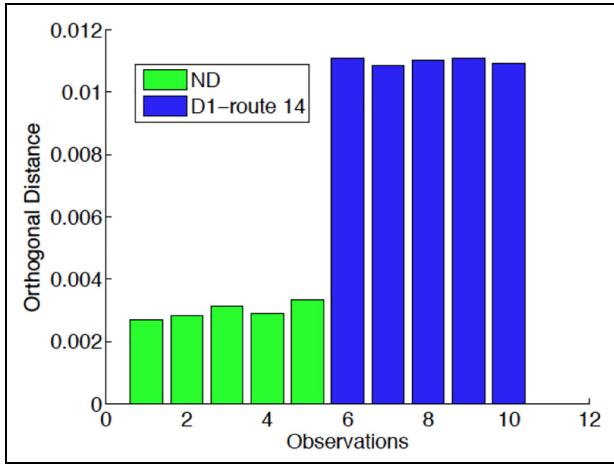
Figure 13. Damage detection using OD, case study 2, 400 kHz, route 1 → 4, damage 1.
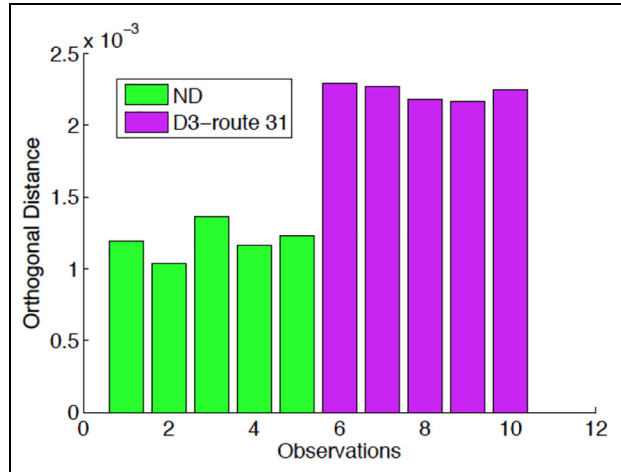
Figure 15. Damage detection using OD, case study 2, 400 kHz, route 1 → 3, damage 3.

Figure 14. Damage detection using OD, case study 2, 400 kHz, route 1 → 2, damage 2.

Figure 16. Damage detection using OD, case study 2, 400 kHz, route 3 → 4, damage 5.

instead of 1 → 3. Figures 17 and 18 show the result of damage detection on these routes. The ODs of three observations randomly selected by each status may be compared. Results are similar to the previous one; although the ODs from observations related to damaged status can be separated from those from undamaged, there is a significant difference for cases where the damage is located on the analyzed route. As in the previous section, the shown results belong to case study 2 and results from case study 1 are omitted as they are similar.[AQ: 3]

Temperature effect on damage detection

As was mentioned in the theoretical background, temperature fluctuation has non-negligible effects on wave propagation, and therefore this must be considered with any damage detection technique. In Figure 19, it may be seen that the peaks of the receiving signal are at different temperatures for the undamaged case in case study 1. The figure clearly shows the magnitude reduction when the temperature is increasing. In addition, this figure clearly shows the velocity decrease (increased time of arrival). According to this figure, signals propagated at higher temperatures arrive later than signals propagated at lower temperatures due to decreasing phase velocities of the propagating wave components as well as slightly increasing the distances that the guided wave should travel in the structure. Furthermore, the time-dependent time shift is clearly evident, the time shift between signal in 25°C and 60°C is increasing by time ($B>A$). The same well-known effects are also seen in case study 2.
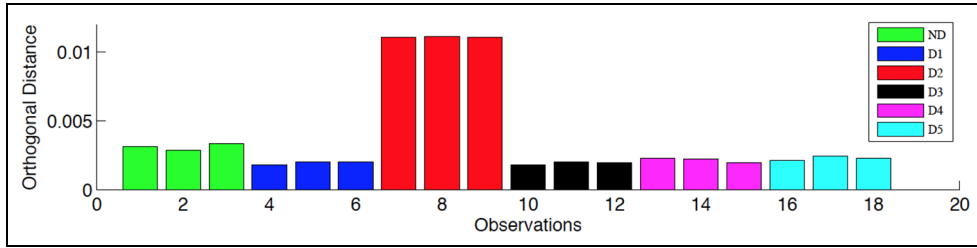
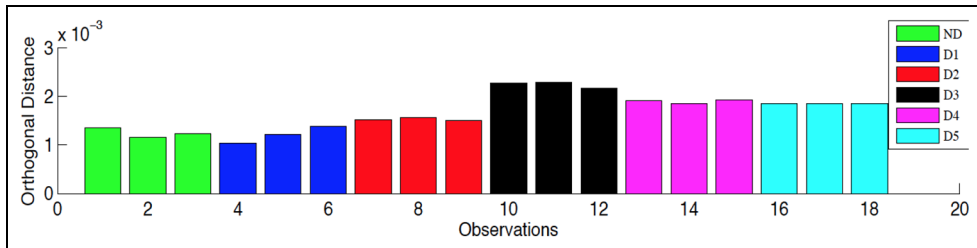**Figure 17.** Damage detection using OD, case study 2, 400 kHz, route 2 → 1, all damages.

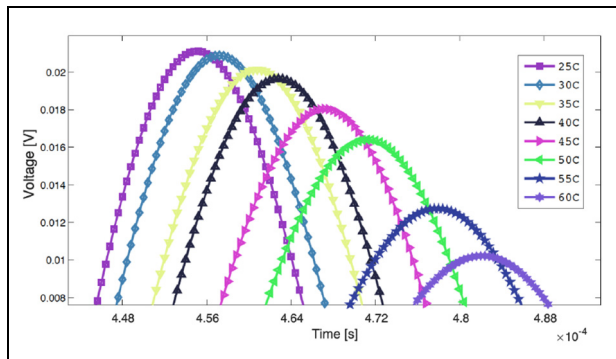**Figure 18.** Damage detection using OD, case study 2, 400 kHz, route 3 → 1, all damages.

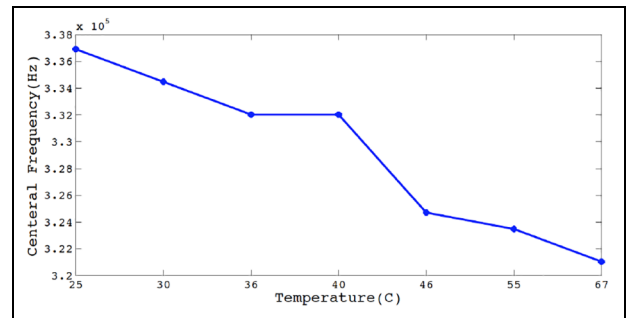**Figure 19.** Propagated wave at different temperatures: case study 1.

Figure 20. Central frequency shift due to temperature fluctuation: case study 2.

Changing the central frequency is another phenomenon that happens when temperature is changed. Figure 20 shows the central frequency change of the received waves with regard to the constant input excitation frequency. As it is seen, central frequency decreases when temperature increases, but the opposite trend happens when the temperature decreases.

Such effects on wave propagation lead to significant drawbacks on damage detection. For instance, OD is clearly affected by temperature change. As it is seen in Figure 21, for the healthy state or undamaged condition, OD is changing relatively and proportionally by the temperature change. Temperature change has a direct effect on OD as increasing the temperature causes OD increase and vice versa. This causes a false
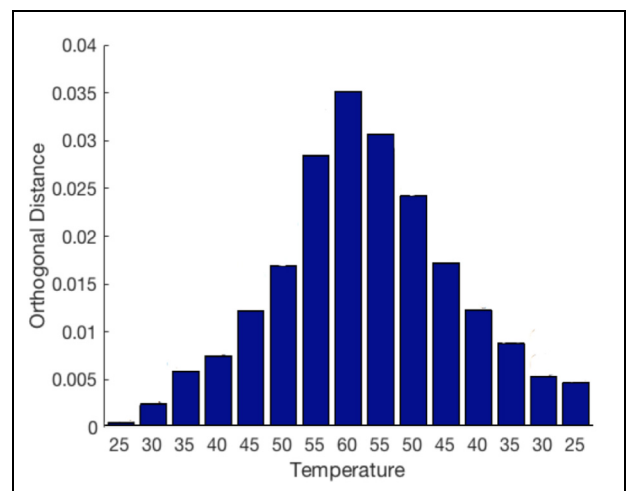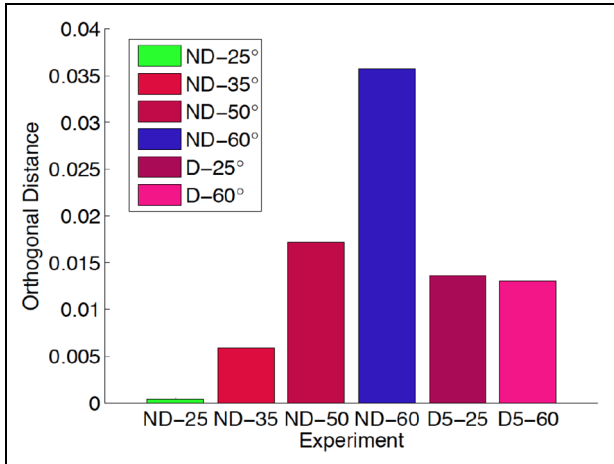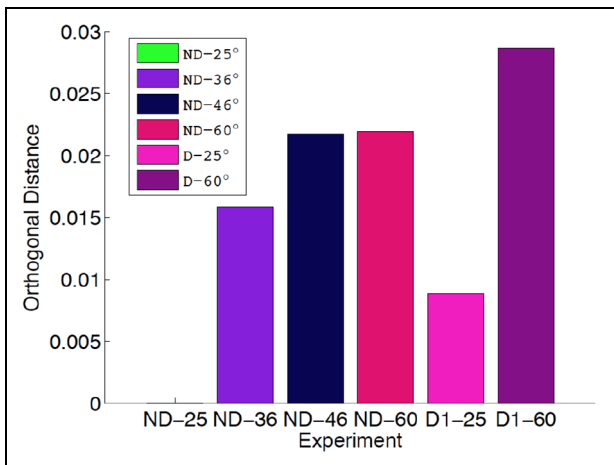

Figure 21. Temperature effect on OD, case study 1, route 1 → 2.

**Figure 22.** Temperature effect on damage detection using OD: case study 1, route 1 → 2.

Figure 23. Temperature effect on damage detection using OD: case study 2, route 1 → 4.

positive alarm when OD is applied as a damage detection feature.

Figures 22 and 23 clearly show that OD from *ND* structure in higher temperature is even more than calculated OD for the damaged structure. This means that temperature changes mask the effect of damage. Both case studies confirm this claim. Results on both case studies affirm that the damage detection goal is not satisfied when there are temperature change in the system. Therefore, temperature compensation should be applied to mitigate the adverse effect of temperature on wave propagation.

Temperature compensation

As it is shown in previous section, temperature change has a significant effect on the propagating signal and
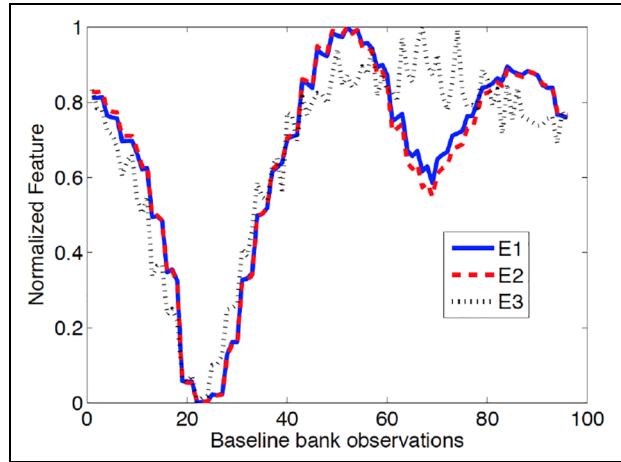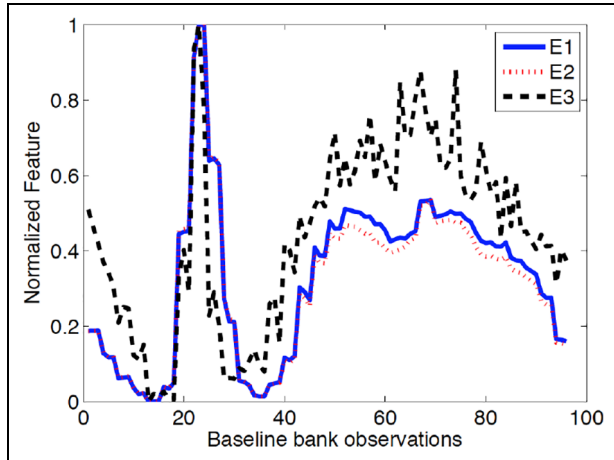

**Figure 24.** Differential features comparison: ND 60°C in case study 1.

the OD. To improve the damage detection reliability, temperature compensation is applied using OBS methodology. To do this, a bank of baselines is recorded on different temperatures in both case studies.

The first case study was subjected to a systematic cyclic change of ambient temperature. The temperature was increased, decreased, increased again, and finally decreased again from 25°C to 60°C with a resolution of 5°C. In a previous work by Mujica et al.,[36] it was shown that in this kind of experimentation, when the structure is subjected to this thermal cycling, the effect on UGWs has a hysteretic character. For instance, the UGW at 45°C when the structure is being heated (e.g. previously it was at 40°C) is significantly different to the UGW at 45°C when the structure is being cooled (e.g. previously it was at 50°C). Therefore, to consider this effect, a baseline bank is created with 96 observations (in healthy status of structure), three by each temperature: 25°C to 60°C (heating), 60°C to 25°C (cooling), 25°C to 60°C (heating again), and 60°C to 25°C (cooling again). The second case study was subjected only to temperature increases: 25, 30, 35, 40, 45, 55, and 67°C. Therefore, a baseline bank is created with 70 observations (in healthy status), 10 by each temperature.

According to OBS, when a new observation from an unknown status and unknown temperature is recorded, it should be compared with the baseline bank to find out the best matched signal (and therefore the optimal baseline) by using equations (13), (14), or (17). For instance, for an observation recorded in a baseline status at 60°C, the differential features are calculated to find the closest observation in the data bank. As it is seen in Figure 24, in the first case-study all the differential features (E1, E2, E3) reach the same minimum, baseline of 60°C. As another example, for an

Figure 25. Differential features comparison: D2 at 35°C in case study 1.
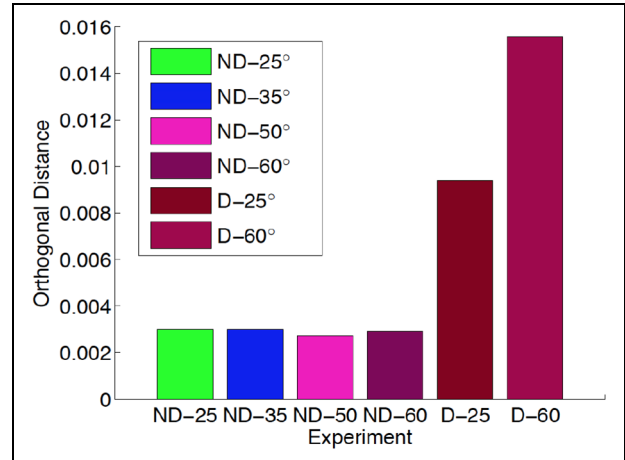
Figure 27. Damage detection using temperature compensation: case study 2, route 1 → 4.
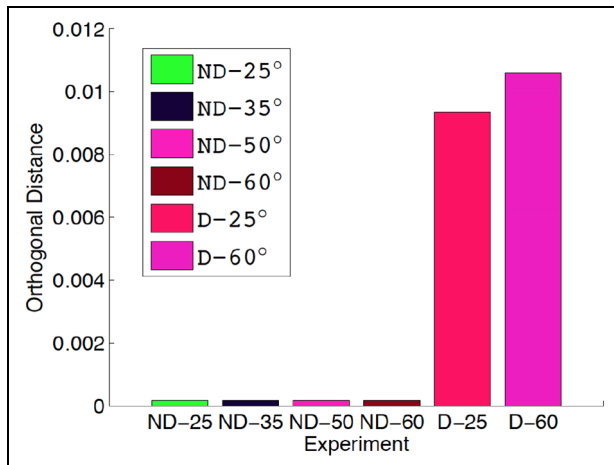
Figure 26. Damage detection using temperature compensation: case study 1, route 1 → 2.

observation at 35°C from structure when D2 is simulated, the baseline with temperature 45°C is selected (see Figure 25). According to both figures, E1, E2, or E3 may have different values along the bank of observations, but usually they select the same observation.

Once a single baseline is selected, the OD is calculated. To do this, a ROBPCA model must be created by each single baseline, since the statistical model cannot be built with few observations (only 3 for case study 1 and 10 for case study 2). Thus, the baseline is statistically enhanced by generating more observations (47 for case study 1 and 40 for case study 2) by adding random normal noise with 95% signal/noise ratio to the gathered measurements. Figures 26 and 27 show the result of this methodology applied on both case studies. As it is clearly seen, observations from the

undamaged condition are not considered damaged anymore; instead, damage detection is successfully done without significant false positive alarms. The proposed methodology minimizes false positives because this is an unsupervised learning method; that is, it does not require any damage data in the training phase. If false negatives were to be considered (by maximizing true-positives), a supervised learning approach would have to be considered where known damage data (also presumably measured at different representative operational/environmental conditions) would have to be included in the training/learning process. Supervised learning techniques are generally much stronger than unsupervised learning techniques, but it is generally true that engineers are not given (or do not have access to) known damage data.

Conclusion

This work shows the ability of using OD of observations from ROBPCA subspace as a damage feature extracted from sparse UGW interrogation when the structure is subject to uniform temperature variations. It is shown that the new feature is capable of distinguishing the observation from damaged structure from the healthy status under limited environmental condition changes. To achieve this, a detection strategy based on OD was presented. Moreover, the PDF of OD is estimated, and it is shown that extreme value distribution could be an acceptable choice. In addition, the specimen is subjected to the temperature changes to analyze the effect of the temperature fluctuation on the performance of the OD feature. It is shown that temperature might have more significant effect on OD

rather than the simulated damage. Therefore, it is necessary to compensate its effects. OBS temperature compensation is utilized to mitigate its effect.

On many structures, thermal gradients (including, for example, very localized "hot spots") are possibly present, and they might not affect the whole structure uniformly; therefore the effects on UGW and subsequently on damage detection are presumably different. It is expected that thermal gradients would induce more information as the waves propagate at changing velocities, but this would nonetheless be compactly captured by ROBPCA. However, this is a hypothesis to be tested and verified, and authors are motivated for future analysis under non-uniform thermal effects.

Finally, there are certainly other operational and environmental conditions that will induce variability in the data as well, but they could not be tested here. As such, it is not yet possible to conclude how they will present themselves in the ROBPCA orthogonalization process. However, it is well known that structures subjected to external loads produce internal strains which change the elastic wave propagation. Its effects are similar to the ones produced by temperature variation. Authors are encouraged to analyze in a future work the strategy based on ROBPCA, OD, and OBS to detect damage on structures subjected to stress.

ORCID iDs

Luis Eduardo Mujica (iD) https://orcid.org/0000-0001-7123-8065

Michael D Todd (iD) https://orcid.org/0000-0002-4492-5887

References

1. Staszewski WJ, Boller C and Tomlinson GR. *Health monitoring of aerospace structures: smart sensor technologies and signal processing*. Chichester: John Wiley & Sons, Inc., 2004.
2. Farrar CR and Worden K. An introduction to structural health monitoring. *Philos T R Soc S: A* 2006; 365(1851): 303–315.
3. Rytter A. *Vibration based inspection of civil engineering structures*. PhD Thesis, Department of Building Technology and Structural Engineering, Aalborg University, Aalborg, 1993.
4. Pawar PM and Ganguli R. *Structural health monitoring using genetic fuzzy systems*. London: Springer-Verlag, 2011.
5. Worden K and Dulieu-Barton JM. An overview of intelligent fault detection in systems and structures. *Struct Health Monit* 2004; 3: 85–98.
6. Michaels JE. Detection, localization and characterization of damage in plates with an *in situ* array of spatially distributed ultrasonic sensors. *Smart Mater Struct* 2008; 17: 035035.
7. Zhou Q, Ning Y, Zhou Q, et al. Structural damage detection method based on random forests and data fusion. *Struct Health Monit* 2013; 12: 48–58.
8. Haynes C, Todd MD, Flynn E, et al. Statistically-based damage detection in geometrically-complex structures using ultrasonic interrogation. *Struct Health Monit* 2013; 12: 141–152.
9. Razi P, Esmaeel RA and Taheri F. Improvement of a vibration-based damage detection approach for health monitoring of bolted flange joints in pipelines. *Struct Health Monit* 2013; 12: 207–224.
10. Nie Z, Hao H and Ma H. Using vibration phase space topology changes for structural damage detection. *Struct Health Monit* 2012; 11: 538–557.
11. Meruane V and Heylen W. Damage detection with parallel genetic algorithms and operational modes. *Struct Health Monit* 2010; 9: 481–496.
12. Poddar B, Bijudas CR, Mitra M, et al. Damage detection in a woven-fabric composite laminate using time-reversed Lamb wave. *Struct Health Monit* 2012; 11: 602–612.
13. Mujica LE, Rodellar J and Vehi J. A review of impact damage detection in structures using strain data. *Int J COMADEM* 2010; 13(1): 3–18.
14. Gharibnezhad F, Mujica LE and Rodellar J. Applying robust variant of principal component analysis as a damage detector in the presence of outliers. *Mech Syst Signal Pr* 2015; 50–51: 467–479.
15. Croxford AJ, Moll J, Wilcox PD, et al. Efficient temperature compensation strategies for guided wave structural health monitoring. *Ultrasonics* 2010; 50: 517–528.
16. Lu Y and Michaels JE. A methodology for structural health monitoring with diffuse ultrasonic waves in the presence of temperature variations. *Ultrasonics* 2005; 43: 717–731.

17. Harley JB and Moura JMF. Scale transform signal processing for optimal ultrasonic temperature compensation. *IEEE T Ultrason Ferr* 2012; 59: 2226–2236.

18. Jolliffe IT. *Principal component analysis* (Springer series in statistics). 2nd ed. New York: Springer-Verlag, 2002.

19. Shlens J. A tutorial on principal component analysis. *Int J Remote Sens*, 2014, https://arxiv.org/abs/1404.1100

20. Smith LI. A tutorial on principal components analysis introduction. *Statistics* 2002; 51: 52.

21. Hubert M, Rousseeuw PJ and Vanden Branden K. ROBPCA: a new approach to robust principal component analysis. *Technometrics* 2005; 47: 64–79.

22. Vanlanduit S, Parloo E, Cauberghe B, et al. A robust singular value decomposition for damage detection under changing operating conditions and structural uncertainties. *J Sound Vib* 2005; 284: 1033–1050.

23. Rousseeuw PJ. Least median of squares regression. *J Am Stat Assoc* 1984; 79: 871–880.

24. Rousseeuw PJ and Van Driessen K. A fast algorithm for the minimum covariance determinant estimator. *Technometrics* 1999; 41: 212–223.

25. Mujica LE, Rodellar J, Fernández A, et al. Q-statistic and T2-statistic PCA-based measures for damage assessment in structures. *Struct Health Monit* 2011; 10(5): 539–553.

26. Sohn H. Effects of environmental and operational variability on structural health monitoring. *Philos T R Soc A* 2007; 365: 539–560.

27. Blaise EJ and Chang FK. Built-in damage detection system for sandwich structures under cryogenic temperatures. In: *Proceedings of the 3rd international workshop on structural health monitoring*, Stanford University, Stanford, CA, 12–14 September 2001.

28. Konstantinidis G, Wilcox PD and Drinkwater BW. An investigation into the temperature stability of a guided wave structural health monitoring system using permanently attached sensors. *IEEE Sens J* 2007; 7: 905–912.

29. Williams RB, Inman DJ and Wilkie WK. Temperature-dependent thermoelastic properties for macro fiber composite actuators. *J Therm Stresses* 2004; 27: 903–915.

30. Raghavan A and Cesnik CES. Effects of elevated temperature on guided-wave structural health monitoring. *J Intel Mat Syst Str* 2008; 19: 1383–1398.

31. Su Z and Ye L. *Identification of damage using lamb waves: from fundamentals to applications* (Lecture notes in applied and computational mechanics). London: Springer-Verlag, 2009.

32. Inman DJ, Farrar CR, Lopes V, et al. *Damage prognosis: for aerospace, civil and mechanical systems.* Chichester: Wiley, 2005.

33. Konstantinidis G, Drinkwater BW and Wilcox PD. The temperature stability of guided wave structural health monitoring systems. *Smart Mater Struct* 2006; 15: 967.

34. Lanza di Scalea F and Salamone S. Temperature effects in ultrasonic Lamb wave structural health monitoring systems. *J Acoust Soc Am* 2008; 124: 161–174.

35. Lilliefors HW. On the Kolmogorov-Smirnov test for normality with mean and variance unknown. *J Am Stat Assoc* 1967; 62: 399–402.

36. Mujica LE, Rodellar J, Vehí J, et al. Extended PCA visualisation of system damage features under environmental and operational variations. *Proc SPIE* 2009; 7286: 72860–72872.